Polymer Testing 120 (2023) 107964

Contents lists available at ScienceDirect

Polymer Testing

journal homepage: www.elsevier.com/locate/polytest

Cellulose nanofibril reinforced functional chitosan biocomposite films

Liguo Qin [a], Yuning Zhang [b], Yanmiao Fan [b], Lengwan Li [c,*]

[a] Key Laboratory of Education Ministry for Modern Design and Rotor-Bearing System, Institute of Design Science and Basic Components, School of Mechanical Engineering, Xi'an Jiaotong University, 710049, PR China
[b] Division of Coating Technology, Department of Fibre and Polymer Technology, KTH Royal Institute of Technology, SE-100 44, Sweden
[c] Department of Fibre and Polymer Technology, Wallenberg Wood Science Center, KTH Royal Institute of Technology, 10044, Stockholm, Sweden

ARTICLE INFO

Keywords:
TEMPO oxidized CNF
Chitosan
Nanocomposites
Biocompatibility
Mechanical properties

ABSTRACT

Recently, chitosan has become attractive due to being biodegradable, biocompatible and renewable. However, the weak mechanical properties of chitosan films limit their large-scale application. In this work, a strategy of blending TEMPO, oxidized CNF (TOCN) and chitosan was developed to fabricate nanocomposite films in order to improve the mechanical properties and maintain biocompatibility. The TOCN/chitosan nanocomposite films exhibited excellent optical transmittance (>85%) and extremely high tensile strength of 235 MPa. The good compatibility of TOCN and chitosan chains, good dispersion of chitosan aggregates and the presence of stiff TOCN crystal domains are the main reasons for getting improved mechanical strength of composite films. The films showed good biocompatible properties based on the cell activity assay results. Furthermore, they were stable in PBS buffer for more than 6 months without significant degradation. The TOCN/chitosan nanocomposite films with these excellent properties could be employed in medical applications.

1. Introduction

In the past decades, the environmental pollution produced by petroleum-based plastic materials has become more and more serious because they are not biodegradable and can remain in the environment for hundreds of years. One possible solution for this issue is to promote bio-based materials that are renewable, biodegradable and abundant in nature. Chitosan is promising in the bio-based materials list because it is a derivative of chitin microfibrils from crustaceans [1]. It has a lot of advantages including biodegradability, biocompatibility and antimicrobial properties [2]. Moreover, it can be easily made into films by simple methods such as solvent casting, electrospraying and direct immersion [3–5].

Chitosan-based films have been explored as promising substrates for various applications. For example, they were applied for removing dyes and metal ions from polluted water [6], used as carriers for drug delivery [7,8] and for applications in regenerative medicine [9]. They were also fabricated into food packaging films that have antibacterial properties [10,11]. However, weak mechanical properties are a major problem of chitosan-based films which limits their further practical application. Intensive efforts have been made to resolve this issue. For instance, some nanofillers such as nano-hydroxyapatite [12], nano metal oxides [13,14], graphene oxide [15,16] and mineral clays [17] show good reinforcement effects on chitosan films. In addition, there are some other additives that can simultaneously enhance the mechanical properties and maintain the biocompatibility of chitosan, such as glycerol [18], xylitol and sorbitol [19], cross-linking agent vanillin [20], hydroxyethyl-cellulose and polyvinyl alcohol (PVA) [21].

Nanocellulose is another biobased, renewable and sustainable material which can easily be fabricated into films [22–24]. Nanocellulose is biodegradable and biocompatible [25] and has excellent functionality [26] and mechanical properties, with intrinsic Young's modulus of 79–220 GPa, ultimate strength of 1.7–7.7 GPa [27]. Herein, nanocellulose can be used as a biobased filler for chitosan. For example, Fernandes et al. used nanofibrillated cellulose (NFC) as reinforcement; the tensile strength of pure chitosan improved from ~50 MPa to ~110 MPa for the composite films [28]. Soni et al. found that TEMPO-oxidized cellulose nanofibrils (TOCN) have strong interactions with chitosan matrix, thus enhancing the mechanical strength, however, the permeability of oxygen and vapor, and optical transmittance were significantly reduced [29]. Tang et al. made transparent chitosan/guar gum/nanocrystalline cellulose composite films; both air barrier and tensile strength properties were improved [30]. These intensive studies show that nanocellulose/chitosan composites have lots of potential for food

* Corresponding author.
E-mail address: lengwan@kth.se (L. Li).

https://doi.org/10.1016/j.polymertesting.2023.107964
Received 17 November 2022; Received in revised form 23 January 2023; Accepted 13 February 2023
Available online 14 February 2023

packaging or medical applications, so the evaluation of their biocompatibility is also needed.

The present approach allows for good TOCN/chitosan co-dispersion and highly transparent and uniform composite nanopapers. Compared to previous reports, the present oxidized cellulose fibers have high negative charge, and went through a high-pressure microfluidizer several times to change fibers into fine nanocellulose fibrils. Rigorous stirring of TOCN/chitosan dilute co-dispersion was carried out to ensure good dispersion. Careful drying of the wet films was taken by sandwiching between woven metal cloths to keep the uniformity of the film. The processing concept allows for good dispersion with efficient interactions on the molecular scale, verified by both rheology and FTIR measurements. The present TOCN/chitosan nanocomposite films show better mechanical properties than in previous reports for TOCN/chitosan based films. The surface morphology and nanoscale structure of the composite films were investigated by AFM and 2D-WAXD. Furthermore, a mouse monocyte cell viability assay was carried out to evaluate the biocompatibility, which has not been reported previously. Overall, the present approach based on biosourced CNF and chitosan, suggest the possibility of manufacturing biocompatible and transparent films for use in medical fields.

2. Materials preparation and characterization methods

2.1. Preparation of TEMPO oxidized CNF

The detailed procedure for making cellulose nanofibrils (CNF) is described in previous studies [31,32]. Briefly, the TEMPO oxidation method was firstly used to oxidize the pulp (Nordic AB). Then, $NaClO_2$ in an acetate buffer was used to further oxidize the pulp to remove the possible remaining lignin. Finally, the oxidized pulp fibers went through a high-pressure homogenizer to fabricate TEMPO-oxidized nanofibrils (TOCN). TOCN has a carboxylate content of ~1 mmol/g and negative charge with ζ-potential of −71 mV. The TOCN had a concentration of ~0.8 wt%.

2.2. Preparation of chitosan dispersion

High purity chitosan (110 kDa, ~75% deacetylated) was obtained from Sigma Aldrich (Sweden). A chitosan solution (1 wt%) was prepared by dissolving chitosan powder (10 g) with acetic acid (2 wt % in deionized water) to obtain a solution of 1000 mL with a final pH of 4. Then, the solution was filtered to remove the undissolved particles.

2.3. Preparation of composite films

Chitosan dispersions were dropped into TOCN dispersion with shearing by an Ultra-Turrax apparatus at a speed of about 10,000 rpm. Note that other shearing speeds are also applicable but the shear-mix time might be different. The concentration of TOCN/chitosan co-dispersion was around 0.1 wt%. The shear-mix process was maintained for 2–5 min until no TOCN aggregates were observed in the co-dispersion. The co-dispersion was then vacuum filtered followed by rapid drying using a Rapid-Köthen machine. The wet cake was sandwiched in woven metal cloths to make sure the heat transfer was quick and uniform. This method is easy to use in a laboratory but probably complicated on an industrial scale. An innovative idea should be developed in order to be able to directly use an internal mixer [33,34] or a twin-screw extruder [35,36]. The designations of TOCN/chitosan nanocomposite film samples are abbreviated based on the percentages of these two components, such as T20C80 (20 wt% TOCN mixed with 80 wt% chitosan), T40C60 (40 wt% TOCN mixed with 60 wt% chitosan).

2.4. Characterization methods

2.4.1. Rheology tests

The rheological tests of TOCN/chitosan co-dispersion at a concentration of 0.3 wt% were carried out using a DHR-2 rotational rheometer from TA Instruments. A frequency sweep from 0.1 to 100 rad/s was conducted on the TOCN/chitosan nanocomposite at controlled stress (1Pa) within the linear viscoelastic range (LVR). The steady-state shear rate was 15 s^{-1} when investigating the effect of temperature.

2.4.2. AFM

The atomic force microscope (AFM) was set to work in tapping mode to provide topographical images of the TOCN/chitosan film surfaces. The AFM tips (Arrow NC-Pt from Nanoworld, Germany) were made of a silicon core coated with a Pt:Ir alloy (radius ~20 nm, resonant frequency 285 kHz). The tapping amplitude was maintained at 30 nm when the tip was in contact with the TOCN/chitosan film surface.

2.4.3. FTIR

The Fourier transform-infrared spectra were recorded using a spectrometer (PerkinElmer Mod. Frontier) equipped with a diamond crystal and attenuated total reflectance (ATR) device. The measurements were carried out at room temperature in the range 4000–600 cm^{-1} (16 scans and 4 cm^{-1} resolution).

2.4.4. SEM

The fracture surface of the films after tensile testing was observed with a Hitachi S-4800 field emission scanning electron microscope (Hitachi, Japan). The films were stuck on a copper tape. Fractured surfaces were coated for 20 s with a thin Pd/Pt layer prior to measurement. The operating working distance was ~8 mm and the accelerating voltage was 1 kV. Energy-dispersive X-ray spectroscopy (EDX) was performed for elemental analysis with an accelerating voltage of 15 kV and a working distance of ~15 mm.

2.4.5. WAXD

2D wide-angle X-ray diffraction measurement (WAXD) was performed using an Anton Paar SAXSpoint 2.0 system equipped with a Cu Kα radiation source, with beam size of 500 μm and wavelength of 1.5418 Å. The detector was an Eiger R 1 M with a tilt detector having a pixel size of 75 × 75 μm. The sample to detector distance was set to 77 mm and the exposure time was 10 min. The sample films were mounted with the X-ray beam parallel to the film surface in the vacuum chamber with a pressure of 1–2 mbar, and the data reduction was conducted using a SAXS analysis package.

Hermans' orientation factor f [37,38] of the lattice plane was calculated based on intensity-azimuthal angle distributions using Equations (1)–(3).

$$f = \frac{3\langle cos^2\,\varphi\rangle - 1}{2} \tag{1}$$

$$\langle cos^2\,\varphi\rangle = \frac{\int_0^{\pi/2} I(\varphi) sin(\varphi) cos^2(\varphi) d\varphi}{\int_0^{\pi/2} I(\varphi) sin(\varphi) d\varphi} \tag{2}$$

where φ is the azimuthal angle, $I(\varphi)$ is the intensity at a given angle φ, and $f = 1$ corresponds to the maximum orientation. The out-of-plane misalignment angle is defined as $\beta = \pm\, \varphi/2$.

The 1D-XRD curves were obtained by integrating the 2D patterns along the q direction. The peak deconvolution method was used to calculate the crystal index. The detailed operation was performed using Originlab software. All the peaks were fitted to a Gaussian function. The

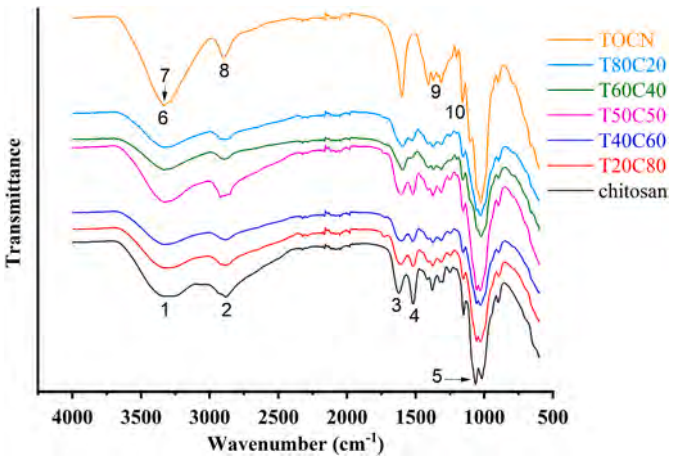

Fig. 1. FTIR spectra of TOCN/chitosan composite sample films. (b).

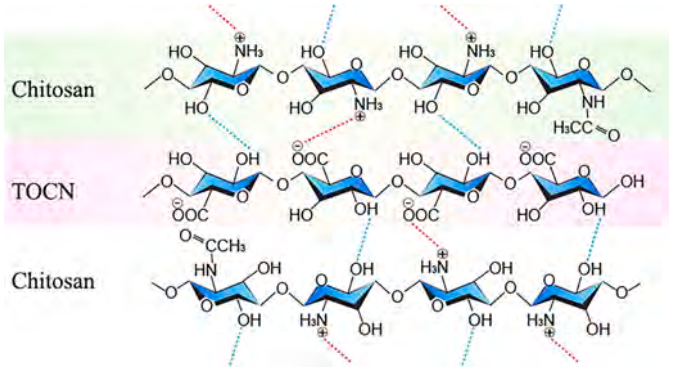

Fig. 2. Molecular structure of TOCN and chitosan nanocomposites.

deconvoluted (1–10)/(110) and (200) peaks were considered as crystalline regions. The peak position of the amorphous region was determined by choosing the q position with minimum intensity between the (1–10)/(110) and (200) peaks. The baseline was determined based on the intensity in the low q region. One example of the deconvoluted peaks is shown in Fig. S1. The deconvoluted crystalline region and amorphous region were further integrated and $A_{crystallinity}$ and $A_{amorphous}$ were obtained. The crystallinity index C is defined as

$$C = A_{crystallinity} \,/\, \left(A_{crystallinity} + A_{amorphous}\right) \tag{3}$$

2.4.6. Transmittance

The optical properties including total transmittance of TOCN/chitosan films were determined using a UV-2550 Shimadzu spectrophotometer with an integrating sphere. The measuring range was from 300 to 800 nm with 0.5 nm intervals.

2.4.7. Degradation test

The TOCN/chitosan films were cut into 10 × 2.5 mm strips and immersed in the 1 M PBS solution. The morphology change of the films was recorded.

2.4.8. Tensile test

The TOCN/chitosan nanocomposite films with a thickness ~30 μm were cut into 70 × 5 mm rectangles. Prior to cutting by a LEICA microtome blade, the films were conditioned in a room with 50 ± 2% relative humidity and 22 ± 1 °C for at least 2 days. Subsequently, the films were stretched in a universal testing machine (Instron 5944, USA), equipped with a 500 N load cell. The gauge length was set to 25 mm and the crosshead speed was 2.5 mm/min, with strain recorded by a video extensometer. At least 5 test pieces from each sample were tested. The Young's modulus was determined by fitting a straight line from the initial elastic deformation region. The yield strength was determined from the intersection point of two linear slope lines of the elastic region and the plastic deforming region. C-fiber, a commercial and medically approved PET fiber mesh (FOV Fabrics AB, Sweden), was used for comparison. It had a weight and thickness of 150 GSM and 0.3–0.4 mm, respectively.

2.4.9. Cellular viability in the leached-out medium

A mouse monocyte (Raw 264.7) cell line was used for evaluating the cellular viability. The cells were cultured at 37 °C in CO_2 (5%) with complete Dulbecco's Modified Eagle Medium (DMEM), supplemented with Fetal Bovine Serum 10% (v/v), L-glutamine (4 mm), penicillin (100 IU/mL) and streptomycin (100 μg/mL).

TOCN/chitosan nanocomposite films were cut into 4 mg pieces and prepared in a sterilized environment, then transferred into 24-well plates and sterilized with UV light for 2 h 1 mL of the complete DMEM were injected into each well and incubated with the samples at room temperature for 24 h to obtain the leached-out medium with certain mass to volume ratio (0.2 mg/mL). Tests were made on triple replicates from each sample.

Cells were collected and seeded into 96-well plates at an initial density of 5×10^4 cells per well. After being pre-cultured for 24 h in the incubator, the old medium was replaced with 100 μL of the leached-out DMEM from the different samples (6 replicate wells for each sample). After 72 h of incubation, 10 μL of Alamar Blue agent was added to each well and the incubation was continued for another 4 h (37 °C, 5% CO_2). Then, the fluorescence intensity was measured at ex/em 560/590 nm with a plate reader (Tecan Infinite M200 Pro, Switzerland).

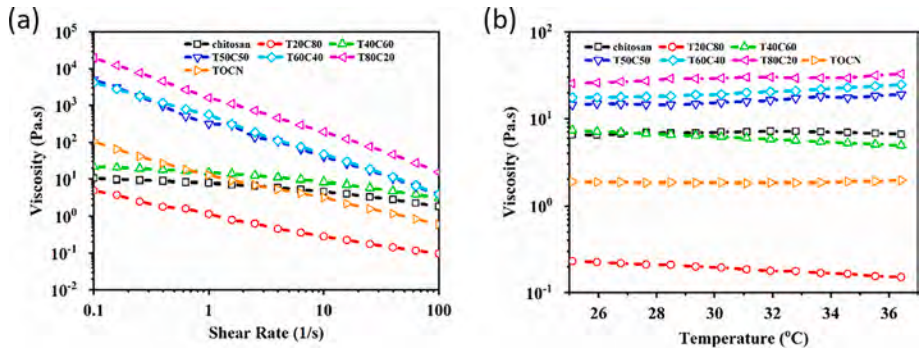

Fig. 3. Viscosity as a function of the (a) shear rate and (b) temperature of different TOCN/chitosan composite dispersions (0.3 wt%). The steady shear rate was 15 s^{-1} over a range of temperatures from 25 to 37 °C.

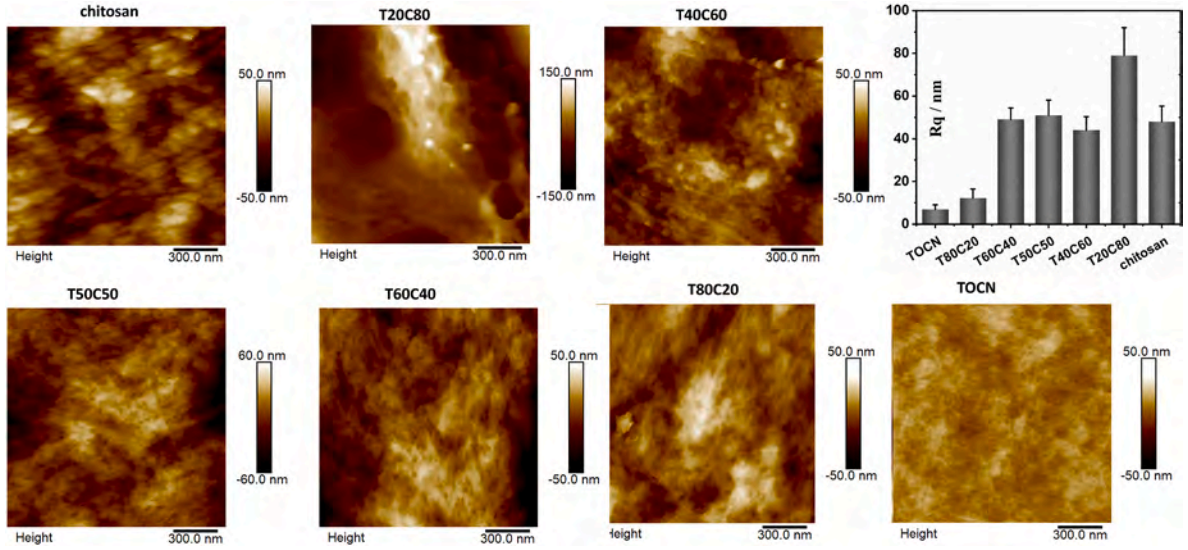

Fig. 4. AFM images of TOCN/chitosan film surface. Sq defines the root mean square value of ordinate values within the definition area. It is equivalent to the standard deviation of heights.

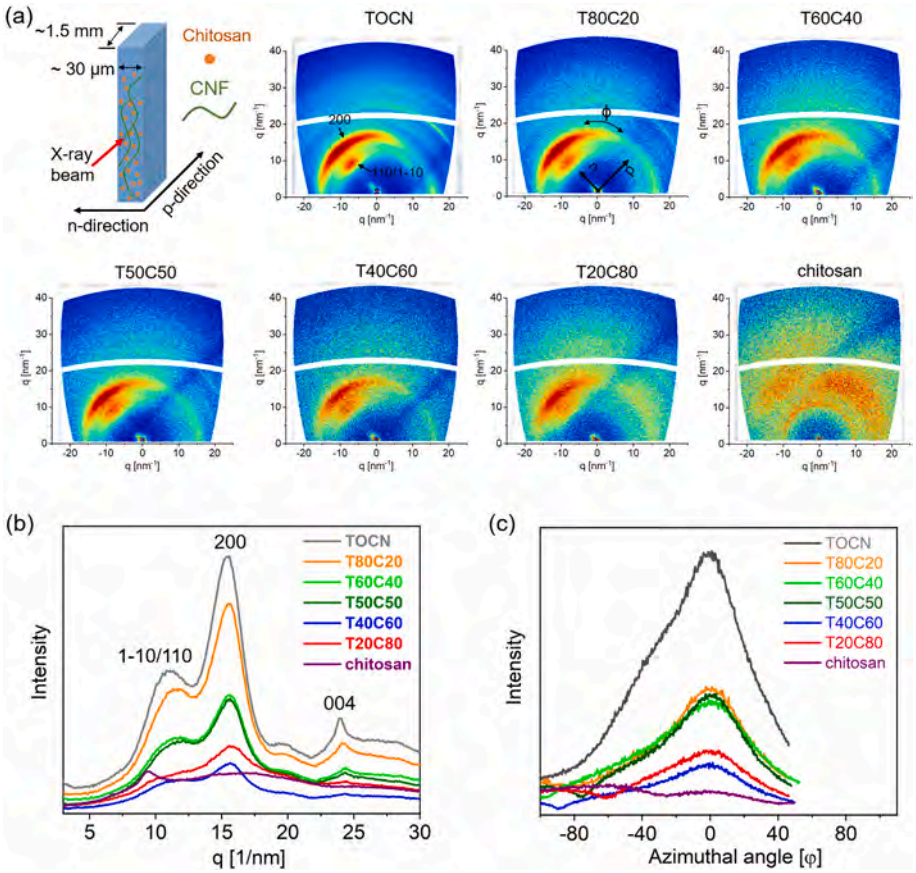

Fig. 5. (a) 2D-WAXD patterns and (b) 1D-WAXD pattern of TOCN/chitosan composites. (c) Intensity as a function of azimuthal angle (φ) curves obtained from CNF 200 crystal spot signals.

3. Results and discussion

The TOCN fibrils had a height of 2–3 nm with a typical length range of 500–700 nm, as reported in previous work [31]. Several cycles of a high-pressure microfluidizer process were applied to ensure the uniformity of the nanofibrils. Both TOCN and chitosan dispersions are colloidally stable in water. The TOCN/chitosan co-dispersion was highly diluted while experiencing rigorous shearing to make sure the mixture was perfect at the molecular length scale, and also to avoid possible aggregation induced by the electrostatic interaction, since the TOCN has negative charge while chitosan has positive charge. The wet cakes after filtration of the co-dispersion were quickly dried in a well-controlled

Table 1
Herman's orientation, misalignment and crystallinity of TOCN/chitosan nanocomposites.

Samples	Herman's orientation	Misalignment	Crystallinity index
TOCN	0.830	9.830	0.272
T80C20	0.829	9.859	0.226
T60C40	0.827	9.934	0.183
T50C50	0.835	9.684	0.176
T40C60	0.831	9.808	0.137
T20C80	0.829	9.864	0.117

drying process. Finally, transparent films with a thickness of ~30 μm were obtained. TOCN/chitosan samples with different composition ratios were produced, with the TOCN reinforcement content ranging from 20 to 80 wt%.

3.1. FTIR analysis

Fig. 1 shows the FITR spectra of composite samples. The absorption bands (peaks) were labelled as numbers in the spectra images. In pristine chitosan film, the broad absorption band (1) is attributed to the stretching of both inter and intra-molecular O–H, $–CH_2OH$ vibrations at 3500–3250 cm^{-1}, and also the stretching of $–NH_2$ (3500–3400 cm^{-1}) and –NH secondary amides vibrations (3300–3280 cm^{-1}). Absorption band 2 (2950–2800 cm^{-1}) comes from the symmetric and asymmetric of C–H vibrations. The sharp peaks at 1624 and 1517 cm^{-1} come from the amide I (stretching of C═O) and amide II vibrations, respectively. Absorption band 5 comes from the C–O stretching at the C-3 position. In pristine TOCN film, the absorption band 6 between 3600 and 3100 cm^{-1} is attributed to the O–H stretching vibration, while the sharp peak 7 at 3338 cm^{-1} mainly comes from the O–H stretching of intramolecular hydrogen bonding. Absorption bands 8, 9 and 10 are C–H stretching, $C–H_2$ stretching and C–O–C stretching vibrations, respectively. In nanocomposite films, the C═O stretch band and 3600-3100 cm^{-1} band regions shows significant change compared to pristine chitosan and TOCN films, indicating the presence of interchain hydrogen bonding or electrostatic interactions between cellulose and chitosan chains as shown in Fig. 2. The C–O stretch band in the C-3 position shows a tiny change, further verifying the interchain hydrogen bonding. In summary, the FTIR results indicate that chitosan and TOCN are compatible with strong interactions of the molecular chains.

3.2. Rheological behavior

The rheological behavior of TOCN/chitosan nanocomposite is strongly dependent on the dispersion state of the TOCN and the interactions between the TOCN and chitosan matrix. In Fig. 3, it was observed that TOCN has a strong impact on the viscosity. The co-dispersion (T20C80) containing the smallest amount of TOCN showed the lowest viscosity, and the addition of 20 wt% TOCN reduced the viscosity compared with the pure chitosan solution (Fig. 3a). This is probably because the fibrils broke some of the granular bulge aggregates. Meanwhile, the number of hydrogen bonding sites is reduced with the cellulose in the chitosan matrix [39]. When the TOCN content was over 40 wt%, the co-dispersions became more viscous, indicating intermixing of TOCN and chitosan chains. The higher viscosity was due to the gradually increasing number of entanglements between the TOCN and chitosan chains. It is widely accepted that a Newtonian fluid has nearly invariant complex viscosity. Similar shear thinning behavior was found for almost all the composite samples (Fig. 3b), the exceptions being chitosan and T40C60, which showed a typical Newtonian viscosity plateau. At higher shear rates, typical non-Newtonian shear--thinning behavior was observed for the other TOCN solution contents, with exponential decrease of viscosity with increasing shear rate. The flow behavior is related to the disentanglement of the chitosan chains. With the synergistic effect of TOCN, electrostatic interaction induced orientation tended to form an anisotropic structure under the action of a shear field.

When measuring the samples with a steady shear rate of 15 s^{-1} from 25 °C to 37 °C, the viscosity was quite constant for all nanocomposite samples, which indicated that the cellulose nanofibril reinforced chitosan hybrid was quite suitable for biomaterials used *in vivo*. Along with the biocompatibility described in the following section, the composite

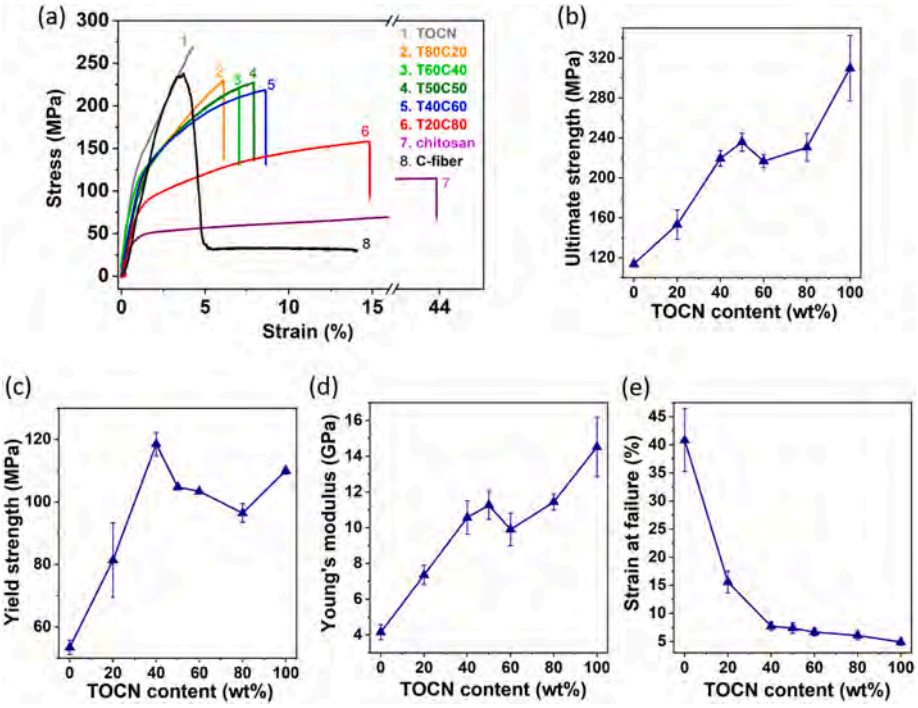

Fig. 6. Mechanical properties of TOCN/chitosan nanocomposite samples: (a) Stress strain curves, (b) Ultimate strength, (c) Yield strength, (d) Young's modulus, (e) Strain at failure. C-fiber is the commercial fabric material.

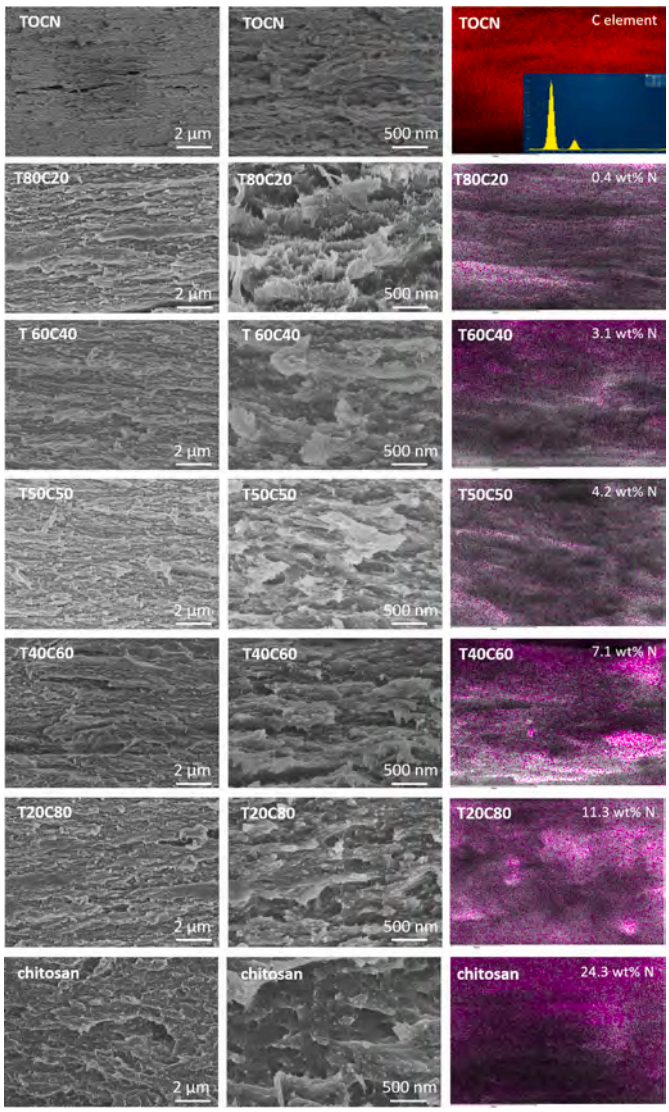

Fig. 7. Morphology of fractured surface and elemental mapping of the nanocomposites.

produced may be a potential candidate for cell adhesion, especially for applications that require both constant fixation and anti-deformation, such as wound dressing materials.

3.3. Morphology of nanocomposite film surfaces

The morphologies of the nanocomposite films were evaluated using AFM. As shown in Fig. 4, TOCN/chitosan with different TOCN contents exhibited a hybrid surface feature. For the pure chitosan, granular bulges were observed due to aggregates formed during the casting/evaporating process. As the TOCN content increased, alignment of nanoscale TOCN fibrils were observed, and granular bulges become less obvious. At lower TOCN concentration (T20C80), rougher features were detected. In T40C60, the chitosan granular bulges were surrounded by the TOCN fibrils. With further increase of TOCN (T50C50), the chitosan granular bulge aggregates disappeared, indicating that the TOCN fibrils can facilitate the dispersion of chitosan. Note that the Rq values (shown in the histogram) decrease when TOCN content exceeded 50%. In the filming process, the interaction between TOCN and chitosan determined the micro features which were detected by AFM. As previously reported [40], well distributed chitosan molecules in aqueous solution were mainly chain-like, and normally had positive charge, which would have strong bonding with a negative nanomaterial, like the TOCN. At a certain proportion, e.g., T40C60 or T80C20, a well hybrid dot and fiber morphology was observed. However, when the ratio of chitosan to TOCN was 2 to 8, the highest Rq was observed. The results indicate that TOCN was strongly connected to chitosan polymer and formed a compound structure.

3.4. Nanostructure of the films

Wide-angle X-ray diffraction (WAXD) measurements were used to elucidate how TOCN and chitosan were organized in the thin film. The measurements were carried out with the incident beam parallel to the film surface. As shown in Fig. 5a, the incident X-ray beam was parallel to the p direction. The neat TOCN film showed typical 1–10/110 and 200 peaks, while in the TOCN/chitosan nanocomposite films these TOCN characteristics remained with the increase of chitosan content, implying that the presence of chitosan does not influence the aggregation structure of TOCN. The pristine chitosan film did not show any diffraction patterns due to the absent of periodic structures. The 2D patterns of TOCN 200 crystal plane were integrated along the azimuthal direction (φ), and the in-plane Herman's orientation factor (>0.8) and out-of-plane misalignments were calculated (Table 1), which indicate that TOCN has high in-plane orientation. The 2D patterns was further integrated along the radial direction, and the 1D-WAXD curves obtained are shown in Fig. 5b. The TOCN peak positions are identical in the TOCN/chitosan nanocomposite films, whereas the intensity decreased due to the decrease of TOCN content. The crystalline index (Table 1) was obtained by calculating the area of amorphous and crystalline regions. The crystalline index was decreased due to the decrease of TOCN content, which corresponds to the weaker mechanical strength of the composite

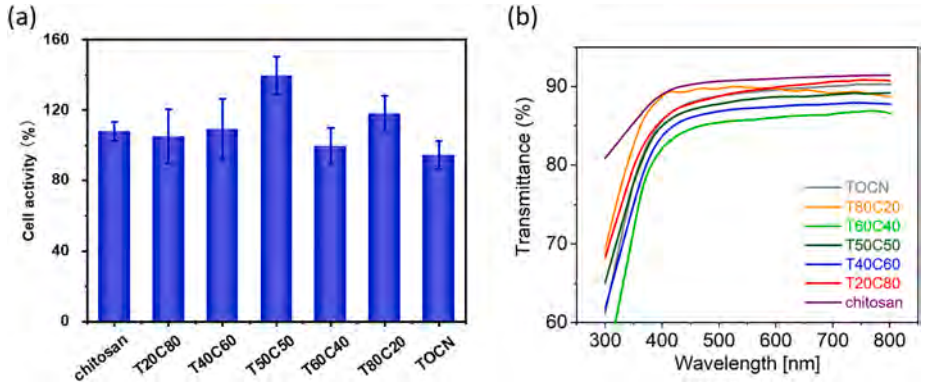

Fig. 8. (a) Cellular viability of Raw264.7 after 72 h incubation in the leached-out medium from different TOCN/chitosan composite films. (b) Transmittance as a function of wavelength of TOCN/chitosan nanocomposite films.

samples with low TOCN content.

3.5. Mechanical properties

The mechanical properties (Fig. 6 and Table S1) of TOCN/chitosan composite films were determined by the tensile tests. The pristine chitosan film showed distinct elastic deformation and plastic deformation regimes. With the increase of TOCN, the films become less ductile, the range of plastic deformation become narrower and the non-linear stress-strain behavior shifted to elastic-brittle-like behavior. Compared to the commercial fabric fibers (C-fiber indicated in Fig. 6), the composite film (e.g., T50C50) showed comparable tensile strength (235.7 MPa *vs.* 226.8 MPa) and Young's modulus (11.3 GPa *vs.* 9.9 GPa), and more than twice the elongation at break (7.4% *vs.* 3.1%). The ultimate strength, yield strength and Young's modulus increased with the increase of TOCN content, while strain to failure decreased. The increase of ultimate strength is probably due to the increase of rigid domains, as suggested by the increased crystallinity obtained from WAXD measurements. The fracture surface was observed by SEM to verify this hypothesis. With the fracture surface change from granular bulges pull-out in pristine chitosan sample to fibril aggregates pull-out in TOCN sample (Fig. 7), the surface roughness become less evident. The EDX images of the blends show a uniform distribution of chitosan in CNF matrix, and the N elements decreased with the increase of TOCN content. This dispersion of chitosan was directly correlated with its effectiveness in improving the mechanical properties of nanocomposite films.

Compared to the CNF/chitosan nanocomposite films reported in previous literature, the integrated mechanical properties of the present composite films are significantly improved, as indicated in Fig. S2 and Table S2. Three possible reasons for the improved mechanical properties are suggested: (1) The good dispersion and inter-mixing of TOCN fibrils and chitosan plays a key role, as verified by the rheology data. (2) Hydrogen bonding and electrostatic interactions are formed between TOCN and chitosan chains, as suggested by FTIR data. (3) The smooth and uniform final films due to a more uniform heat transfer process during drying.

3.6. Biocompatibility and optical transmittance

The cytotoxicity of the materials was investigated in order to explore possible *in vivo* applications and drug delivery of TOCN/chitosan composite films. The TOCN/chitosan composite films were incubated in the complete DMEM medium to obtain the leached-out medium which was supposed to contain toxic substances if they existed [41]. Mouse monocyte Raw264.7 was cultured with the leached-out medium for 72 h and the viability determined with AlamarBlue assay. The TOCN/chitosan nanocomposite films were found to be non-toxic (mitochondrial activity >70%) against Raw264.7 cells, exhibiting weak cytotoxicity for all the compositions (Fig. 8a). These results confirm that the materials are promising for biocompatible nanocomposite systems. Especially for the T50C50 sample, cell growth was stimulated, indicating that equal amounts of TOCN and chitosan is the best for cell growth. Furthermore, all the nanocomposite films were optically transparent and showed high total transmittance of over 85% at 500–800 nm wavelength range (Fig. 8b), which is due to the uniform TOCN fibril size and distribution at the nanoscale. Various transparent film materials showed improved effects for disease treatments, e.g., eye treatment as functional contact lenses [42,43]. The present TOCN and chitosan composite materials can potentially be used as a contact lens for ocular drug release due to their high optical transmittance as well as the higher stability, as indicated in Fig. S3.

4. Conclusions

In summary, TOCN/chitosan nanocomposite films with significantly improved physicochemical properties were prepared via carefully controlled processing of the TOCN and chitosan dispersion. The main findings are listed as: (1) All the nanocomposite films maintained good transparency with the addition of TOCN. The viscosity of the hybrid suspensions increased and remained constant at different temperatures, which indicates that the nanocomposites are suitable for *in vivo* applications. (2) Chitosan and TOCN chains showed good compatibility with strong hydrogen bonding interactions. Benefiting from the good dispersion and higher crystallinity, the nanocomposite films exhibited improved mechanical properties compared to the neat chitosan films and commercial fabric fibers used for wound healing. (3) The nanocomposite films showed excellent biocompatibility, verified by the non-toxic behavior against mouse monocyte Raw264.7 cells and excellent stability in PBS buffer, indicating their potential use in biomedical applications, such as contact lens, drug release, etc. It also shows the possibility to replace current commercial wound healing materials. Overall, the addition of nanocellulose can overcome chitosan's main mechanical weakness and lead to a total biocompatible nanocomposite with the advantages of being obtained from bio-sources, contributing to sustainability and environmental safety concerns.

Author statement

Liguo Qin: Conceptualization; Data curation; Formal analysis; Funding acquisition; Investigation; Methodology; Roles/Writing - original draft., **Yuning Zhang:** Data curation; Formal analysis., **Yanmiao Fan:** Data curation; Formal analysis., **Lengwan Li:** Conceptualization; Data curation; Formal analysis; Funding acquisition; Investigation; Methodology; Project administration; Supervision; Roles/Writing - original draft; Writing - review & editing.

Declaration of competing interest

The authors declare that they have no known competing financial interests or personal relationships that could have appeared to influence the work reported in this paper.

Data availability

Data will be made available on request.

Acknowledgements

The authors acknowledge the National Natural Science Foundation of China (51975458 and 51605370), the financial support from the China Scholarship Council, China Postdoctoral Science Foundation funded project (2020M673377 and 2020T130510) and the Natural Science Fund of Shaanxi Province (2020JM-010). The authors acknowledge funding from the Swedish Research Council, project 2021–03882, and the Knut and Alice Wallenberg Foundation through Wallenberg Wood Science Center and the Biocomposites program at the KTH Royal Institute of Technology. Treesearch Research Infrastructure is acknowledged for their financial support of the WAXD analysis at Research Institutes of Sweden (RISE). The authors would also like to thank Assoc. Prof. Anita Teleman from RISE for the help in conducting the WAXD measurements. The authors acknowledge the constructive comments from Prof. Lars A. Berglund.

Appendix A. Supplementary data

Supplementary data to this article can be found online at https://doi.org/10.1016/j.polymertesting.2023.107964.

References

[1] S. Kou, L.M. Peters, M.R. Mucalo, Chitosan: a review of sources and preparation methods, Int. J. Biol. Macromol. 169 (2021) 85–94.

[2] M.E. Abd El-Hack, M.T. El-Saadony, M.E. Shafi, N.M. Zabermawi, M. Arif, G. E. Batiha, A.F. Khafaga, Y.M. Abd El-Hakim, A.A. Al-Sagheer, Antimicrobial and antioxidant properties of chitosan and its derivatives and their applications: a review, Int. J. Biol. Macromol. 164 (2020) 2726–2744.
[3] T. Freier, H.S. Koh, K. Kazazian, M.S. Shoichet, Controlling cell adhesion and degradation of chitosan films by N-acetylation, Biomaterials 26 (2005) 5872–5878.
[4] M. Kurakula, N. Raghavendra Naveen, Electrospraying, A facile technology unfolding the chitosan based drug delivery and biomedical applications, Eur. Polym. J. 147 (2021), 110326.
[5] Y. Luo, X. Pan, Y. Ling, X. Wang, R. Sun, Facile fabrication of chitosan active film with xylan via direct immersion, Cellulose 21 (2014) 1873–1883.
[6] E. Salehi, P. Daraei, A. Arabi Shamsabadi, A review on chitosan-based adsorptive membranes, Carbohydr. Polym. 152 (2016) 419–432.
[7] S. Rodrigues, M. Dionísio, C.R. López, A. Grenha, Biocompatibility of chitosan carriers with application in drug delivery, J. Funct. Biomater. 3 (2012) 615–641.
[8] W. Deng, Y. Tang, J. Mao, Y. Zhou, T. Chen, X. Zhu, Cellulose nanofibril as a crosslinker to reinforce the sodium alginate/chitosan hydrogels, Int. J. Biol. Macromol. 189 (2021) 890–899.
[9] F.S. Rezaei, F. Sharifianjazi, A. Esmaeilkhanian, E. Salehi, Chitosan films and scaffolds for regenerative medicine applications: a review, Carbohydr. Polym. 273 (2021), 118631.
[10] B. Tian, Y. Liu, Chitosan-based biomaterials: from discovery to food application, Polym. Adv. Technol. 31 (2020) 2408–2421.
[11] P.K. Dutta, S. Tripathi, G.K. Mehrotra, J. Dutta, Perspectives for chitosan based antimicrobial films in food applications, Food Chem. 114 (2009) 1173–1182.
[12] P. Roy, R.R.N. Sailaja, Chitosan–nanohydroxyapatite composites: mechanical, thermal and bio-compatibility studies, Int. J. Biol. Macromol. 73 (2015) 170–181.
[13] S. Ullah, I. Zainol, R.H. Idrus, Incorporation of zinc oxide nanoparticles into chitosan-collagen 3D porous scaffolds: effect on morphology, mechanical properties and cytocompatibility of 3D porous scaffolds, Int. J. Biol. Macromol. 104 (2017) 1020–1029.
[14] R.T. De Silva, M.M.M.G.P.G. Mantilaka, S.P. Ratnayake, G.A.J. Amaratunga, K.M. N. de Silva, Nano-MgO reinforced chitosan nanocomposites for high performance packaging applications with improved mechanical, thermal and barrier properties, Carbohydr. Polym. 157 (2017) 739–747.
[15] J. Ahmed, M. Mulla, Y.A. Arfat, L.A. Thai T, Mechanical, thermal, structural and barrier properties of crab shell chitosan/graphene oxide composite films, Food Hydrocolloids 71 (2017) 141–148.
[16] D. Han, L. Yan, W. Chen, W. Li, Preparation of chitosan/graphene oxide composite film with enhanced mechanical strength in the wet state, Carbohydr. Polym. 83 (2011) 653–658.
[17] M.Z. Elsabee, E.S. Abdou, Chitosan based edible films and coatings: a review, Mater. Sci. Eng. C 33 (2013) 1819–1841.
[18] Y. Ma, L. Xin, H. Tan, M. Fan, J. Li, Y. Jia, Z. Ling, Y. Chen, X. Hu, Chitosan membrane dressings toughened by glycerol to load antibacterial drugs for wound healing, Mater. Sci. Eng. C 81 (2017) 522–531.
[19] M. Matet, M.-C. Heuzey, E. Pollet, A. Ajji, L. Avérous, Innovative thermoplastic chitosan obtained by thermo-mechanical mixing with polyol plasticizers, Carbohydr. Polym. 95 (2013) 241–251.
[20] Z.-H. Zhang, Z. Han, X.-A. Zeng, X.-Y. Xiong, Y.-J. Liu, Enhancing mechanical properties of chitosan films via modification with vanillin, Int. J. Biol. Macromol. 81 (2015) 638–643.
[21] M.I. Wahba, Enhancement of the mechanical properties of chitosan, J. Biomater. Sci. Polym. Ed. 31 (2020) 350–375.
[22] T. Liu, Z. Liu, Z. Fang, J. Zhang, S. Gong, J. Li, An ultrastrong, reversible thermochromic film based on TEMPO-oxidized nanofibrillated cellulose, Compos. B Eng. 224 (2021), 109191.
[23] Y. Hua, T. Chen, Y. Tang, Preparation and characterization of nanocomposite films based on different ratios of cellulose nanocrystal and cellulose nanofiber, Ind. Crop. Prod. 179 (2022), 114686.
[24] Y. Song, T. Wu, J. Bao, M. Xu, Q. Yang, L. Zhu, Z. Shi, G.-H. Hu, C. Xiong, Porous cellulose composite aerogel films with super piezoelectric properties for energy harvesting, Carbohydr. Polym. 288 (2022), 119407.
[25] A. Subhedar, S. Bhadauria, S. Ahankari, H. Kargarzadeh, Nanocellulose in biomedical and biosensing applications: a review, Int. J. Biol. Macromol. 166 (2021) 587–600.
[26] Y. Song, Z. Shi, G.-H. Hu, C. Xiong, A. Isogai, Q. Yang, Recent advances in cellulose-based piezoelectric and triboelectric nanogenerators for energy harvesting: a review, J. Mater. Chem. 9 (2021) 1910–1937.
[27] T.C. Mokhena, E.R. Sadiku, M.J. Mochane, S.S. Ray, M.J. John, A. Mtibe, Mechanical properties of cellulose nanofibril papers and their bionanocomposites: a review, Carbohydr. Polym. 273 (2021), 118507.
[28] S.C.M. Fernandes, C.S.R. Freire, A.J.D. Silvestre, C. Pascoal Neto, A. Gandini, L. A. Berglund, L. Salmén, Transparent chitosan films reinforced with a high content of nanofibrillated cellulose, Carbohydr. Polym. 81 (2010) 394–401.
[29] B. Soni, E.B. Hassan, M.W. Schilling, B. Mahmoud, Transparent bionanocomposite films based on chitosan and TEMPO-oxidized cellulose nanofibers with enhanced mechanical and barrier properties, Carbohydr. Polym. 151 (2016) 779–789.
[30] Y. Tang, X. Zhang, R. Zhao, D. Guo, J. Zhang, Preparation and properties of chitosan/guar gum/nanocrystalline cellulose nanocomposite films, Carbohydr. Polym. 197 (2018) 128–136.
[31] L. Li, L. Maddalena, Y. Nishiyama, F. Carosio, Y. Ogawa, L.A. Berglund, Recyclable nanocomposites of well-dispersed 2D layered silicates in cellulose nanofibril (CNF) matrix, Carbohydr. Polym. 279 (2022), 119004.
[32] Y. Kobayashi, T. Saito, A. Isogai, Aerogels with 3D ordered nanofiber skeletons of liquid-crystalline nanocellulose derivatives as tough and transparent insulators, Angew Chem. Int. Ed. Engl. 53 (2014) 10394–10397.
[33] W.-Y. Ji, T.-T. Li, S.-B. Cheng, L.-F. Feng, X.-P. Gu, C.-L. Zhang, G.-H. Hu, Two antagonistic effects of flow/mixing on reactive polymer blending, AIChE J. 68 (2022), e17835.
[34] L.-F. Feng, G.-H. Hu, Reaction kinetics of multiphase polymer systems under flow, AIChE J. 50 (2004) 2604–2612.
[35] L. Chen, Z. Pan, G.-H. Hu, Residence time distribution in screw extruders, AIChE J. 39 (1993) 1455–1464.
[36] X.-M. Zhang, Z.-B. Xu, L.-F. Feng, X.-B. Song, G.-H. Hu, Assessing local residence time distributions in screw extruders through a new in-line measurement instrument, Polym. Eng. Sci. 46 (2006) 510–519.
[37] P.H. Hermans, P. Platzek, Beiträge zur Kenntnis des Deformationsmechanismus und der Feinstruktur der Hydratzellulose, Kolloid Z. 88 (1939) 68–72.
[38] L. Medina, Y. Nishiyama, K. Daicho, T. Saito, M. Yan, L.A. Berglund, Nanostructure and properties of nacre-inspired clay/cellulose nanocomposites—synchrotron X-ray scattering analysis, Macromolecules 52 (2019) 3131–3140.
[39] M.M. Villar-Chavero, J.C. Domínguez, M.V. Alonso, M. Oliet, F. Rodriguez, Chitosan-reinforced cellulosic bionogels: viscoelastic and antibacterial properties, Carbohydr. Polym. 229 (2020), 115569.
[40] L. Qin, H. Dong, Z. Mu, Y. Zhang, G. Dong, Preparation and bioactive properties of chitosan and casein phosphopeptides composite coatings for orthopedic implants, Carbohydr. Polym. 133 (2015) 236–244.
[41] V. Granskog, S. García-Gallego, J. von Kieseritzky, J. Rosendahl, P. Stenlund, Y. Zhang, S. Petronis, B. Lyvén, M. Arner, J. Håkansson, M. Malkoch, High-Performance thiol–ene composites unveil a new era of adhesives suited for bone repair, Adv. Funct. Mater. 28 (2018), 1800372.
[42] A. Than, C. Liu, H. Chang, P.K. Duong, C.M.G. Cheung, C. Xu, X. Wang, P. Chen, Self-implantable double-layered micro-drug-reservoirs for efficient and controlled ocular drug delivery, Nat. Commun. 9 (2018) 4433.
[43] F.H. Nasr, S. Khoee, M.M. Dehghan, S.S. Chaleshtori, A. Shafiee, Preparation and evaluation of contact lenses embedded with polycaprolactone-based nanoparticles for ocular drug delivery, Biomacromolecules 17 (2016) 485–495.